Research Article

ZEBRA OPTIMIZATION ALGORITHM FOR POWER CONDITIONER WITH FRACTIONAL ORDER PID CONTROLLER FOR POWER QUALITY IMPROVEMENT IN PHOTOVOLTAIC ENERGY SYSTEM

Ahmed M. MAKLAD[1,*], *Gamal A. MORSY*[2], *Heba A. KHATTAB*[2], *Ragab A. AMER*[2]

[1]North Cairo Power Plant, Cairo Electricity Production Company, Ministry of Electricity and Renewable Energy, Egypt
[2]Department of Electrical Engineering, Faculty of Engineering, Menoufia University, Shebin El-Kom, Egypt

Ahmed.Mohamed557@sh-eng.menofia.edu.eg, heba.khatab@sh-eng.menofia.edu.eg, jamal.mohamed@sh-eng.menofia.edu.eg, ragaba7med@sh-eng.menofia.edu.eg

[*]Corresponding author: Ahmed M. Maklad; Ahmed.Mohamed557@sh-eng.menofia.edu.eg

DOI: 10.15598/aeee.v23i2.250202

Article history: Received Feb 3, 2025; Revised Apr 04, 2025; Accepted Apr 14, 2025; Published Jun 30, 2025.

Abstract. *The growing use of advanced equipment in modern systems, such as electronic devices and drives, has led to a decline in power quality (PQ), causing malfunctions in sensitive loads. Additionally, the integration of renewable energy sources into the power grid significantly impacts the PQ of the electrical system. To address these effects on voltage stability and harmonic distortion, the unified power flow controller (UPFC) series compensator has proven to be a highly effective solution. This study focuses on using the UPFC to mitigate PQ issues related to renewables, including voltage sag, swell, harmonics, and fault conditions. The UPFC is controlled by a fractional order proportional integral derivative (FOPID) controller, which uses the improved zebra optimization algorithm (ZOA) to determine optimal gain values under various PQ scenarios. Furthermore, three comparative assessments of different optimization approaches are conducted to achieve the desired performance and power of the proposed UPFC. The results showed that the proposed ZOA approach compared with WOA and PSO yielded the shortest computing time of 173.554, 257.544, and 382.405 seconds and achieved an objective function value of 2.371, 2.387, and 2.398, respectively. The effectiveness of the proposed strategy is validated using the MATLAB/Simulink platform, with results showing significant improvements in voltage stability and harmonic reduction.*

Keywords

Power quality, unified power flow controller, harmonic distortion, renewables, zebra optimization algorithm (ZOA).

1. Introduction

The growing reliance on sophisticated and sensitive technologies, including electronic systems and industrial drives, has paralleled advancements in renewable energy solutions such as microturbines, wind turbines, and photovoltaic (PV) systems [1]. Their incorporation into low-voltage microgrids has created a demand for effective monitoring systems to manage power quality (PQ) challenges [2]. Deteriorating PQ levels, marked by heightened energy losses and disruptions in critical, sensitive equipment, underscore the urgency of addressing these issues [3]. Economically driven factors linked to such technologies are central to PQ disturbances, emphasizing the need for solutions that bal-

ance technical and consumer priorities. Sensitive devices are especially susceptible to introducing harmonics into the power supply, triggering PQ anomalies like voltage fluctuations, imbalances, and waveform distortions. Consequently, developing methodologies to accurately measure, analyze, and mitigate power quality concerns is essential to maintaining grid stability within standardized thresholds [4].

Power quality (PQ) challenges, including disruptions, voltage sags, harmonic distortions, and voltage swells, arise from the intermittent changes in environmental conditions affecting renewable energy sources (RESs) and the dynamic behavior of loads [5]. Addressing these challenges is crucial for enhancing the reliability and resilience of independent microgrid systems. In standalone microgrids, Flexible Alternating Current Transmission Systems (FACTS) devices, such as filters and specialized PQ equipment, play a key role in mitigating PQ issues [6, 7]. These devices, including series and shunt compensators, are integrated into microgrids to manage and correct voltage irregularities. However, effectively managing compensators can be challenging due to their dependence on controller outputs [8]. Various control strategies, such as Fractional-Order Proportional Integral Derivative (FOPID) and Fuzzy Logic (FL) controllers, have been employed to address PQ concerns [9–11].

Numerous research efforts have been made to address power quality (PQ) challenges in integrated systems, particularly focusing on renewable energy sources (RES) and microgrids (μGs) [12, 13]. Scholars have explored various methods and control techniques to enhance the efficiency and resilience of these setups, presenting multiple models to mitigate PQ issues. In the realm of Flexible Alternating Current Transmission Systems (FACTS), the Unified Power Flow Conditioner (UPFC) outperforms in multifunctionality by combining the D-STATCOM and dynamic voltage restorer (DVR) [14]. The UPFC effectively achieves key objectives such as improving power factor, reducing total harmonic distortion (THD), enhancing voltage profiles, and generally boosting PQ across the system [15]. Compared to traditional grid configurations, the reliability of the grid-associated SPV-WES-BESS-EVs system increased when Battery Energy Storage Systems (BESS) and Electric Vehicles (EVs) were integrated using Fuzzy Logic Control (FLC) to deliver higher PQ [16]. To reduce total harmonic distortion (THD) and improve power factor, the firefly optimization method, which mimics predator-prey interactions, was used to determine optimal shunt filter parameters and proportional integral (PI) controller gain values [17, 18]. Additionally, an Ant Colony Algorithm was employed to select PI controller gains for the shunt filter, effectively decreasing THD under various load conditions [19]. A novel approach was introduced to enhance the power factor (PF) of a five-level UPFC and maximize THD by combining FLC and neural network control (NNC) [20]. PQ issues in the distribution network connected to a microgrid were addressed by implementing UPFC, which targets voltage imbalances and current harmonics [21]. Additionally, an AI-based neuro-fuzzy (NF) controller was recommended to improve system usage and efficiency [22]. To tackle PQ problems in a distribution system, a unique control technique integrating the Moth Flame and Bat algorithms was developed, aiming to reduce inaccuracies caused by supply voltage variations. This method also lowered the operating costs of renewable energy sources (RES) by adjusting gain settings [23]. Furthermore, a novel strategy for a shunt active power filter (SHAPF) was proposed, combining neural networks (NN) with Enhanced Efficient Global Optimization to improve PQ in the distribution system and reduce current disruptions [24]. It was proposed a firefly algorithm-optimized artificial neural network controller (FF-ANNC) for the shunt active filter and a proportional-integral controller (PI-C) for the series active filter in the UPQC [25]. The UPQC is integrated with a solar energy system and battery energy storage system, employing a boost converter and buck-boost converters for power management.

This research introduces a novel approach that employs an optimization-driven Fractional-Order proportional integral derivative controller (FOPID) to enhance power quality (PQ) in interconnected microgrid systems, with a particular focus on the UPFC. The zebra optimization algorithm (ZOA) method is used to fine-tune the controller parameters. The main objective of this study is to improve PQ in a hybrid renewable energy sources (RES) grid-connected nonlinear distribution system by utilizing the proposed FOPID control method for UPFCs.

The key contributions of this research can be outlined as:

- Establishing a hybrid RES that integrates a load model, connecting a UPFC to supervise PQ.
- Utilizing the FOPID controller to generate pulse signals for the UPFC scheme switches by matching real and reference values.
- Fine-tuning the parameters of the FOPID controller using the ZOA algorithm.
- Evaluating the performance of the proposed model across various PQ scenarios, involving sags, swells, faults, and harmonics.
- Conducting a comparative investigation among manual gain adjustment and tuning facilitated by the ZOA algorithm.

The rest of the manuscript is structured as follows:

- Section 2 elaborates on the overall structure and methodology of the research.
- Section 3 presents the control policy for the proposed UPFC system.
- Section 4 delineates the problem formulation and the ZOA algorithm utilized.
- Section 5 provides an assessment of the model's performance.
- Finally, Section 6 offers a summary of the overarching conclusions.

2. System investigation

Figure 1 depicts a sample study of a distribution system, featuring an 22 kV, 50 Hz AC utility connected to a PV and wind microgrid (μG). Two feeders are linked to the point of common coupling (Vpcc) via transformer windings T3 and T4, with ratings of 750 kVA and 1000 kVA, respectively. Feeder 1 is connected to non-sensitive loads with a 500 kVA rating. Feeder 2 is connected through a UPFC circuit to AC industrial loads with a 750 kVA rating and a power factor (PF) of 0.7 lagging [26].

2.1. Photovoltaic

One possible way to estimate the output power of PV generation is given through the following expression [27–29]:

$$P_{PV} = \eta_g N_{PV} A_m G_i \tag{1}$$

Here, η_g represents the PV generation efficiency, and N_{PV} denotes the number of PV modules. A_m and G_i correspond to the utilized area of a single module (m^2) and the overall incidence of irradiance on the tilted plane (W/m^2), respectively [30–34]. The η_g can be conveyed as:

$$\eta_g = \eta_r \eta_{pt}[1 - \beta_t(T_c - T_r)] \tag{2}$$

In Equation (2), η_r represents the PV reference efficiency, while η_{pt} corresponds to the efficiency of the tracking power appliance when utilizing maximum power point tracking, both taking a value of 1. T_r and T_c signify the reference and PV cell temperatures in degrees Celsius (°C), respectively. β_t signifies the efficiency temperature factor [35, 36].

3. UPFC modelling

The UPFC is built up by two inverters linked to a single dc capacitor. The series converter is linked via a series transformer, and the shunt converter is linked in parallel to the VL2. The series and shunt converters act as voltage and current sources, respectively [27,37]. The schematic layout of UPFC in this work is shown on Fig. 2. Parallel power management and PQ control are made possible by the grid connections for the EV, BESS, PV, and WT. The prime role of series filter's, Dynamic Voltage Restorer (DVR), is to solve voltage issues originated at grid by delivering the necessary injecting voltage (V_{inj}) and the appropriate selection of series filter circuit via the interface transformer. Likewise, shunt filter circuit is used to link the shunt filter to the grid. The SHAPF is increasing compensating currents to reduce the current's harmonic content [38, 39].

3.1. Shunt controller

The control strategy of the UPFC's-shunt power filter (SPF) follows switching criteria:

Switching conditions for S_3 = on and S_4 = off are given as

$$v_A(t) - v_{A,min} - \left[\frac{k_A}{\frac{v_{DC}}{2} - v_A(t)}\right] i_C^2(t) \leq 0 \tag{3}$$

$$i_C(t) \leq 0 \tag{4}$$

Switching conditions for S_3 = off and S_4 = on are given as

$$v_A(t) - v_{A,max} + \left[\frac{k_A}{\frac{v_{DC}}{2} + v_A(t)}\right] i_C^2(t) \geq 0 \tag{5}$$

$$i_C(t) \geq 0 \tag{6}$$

In this context, k_A represents a fixed value determined by $k_A = \frac{L_A}{2C_A}$. The values $v_{A,min}$ and $v_{A,max}$ indicate the lower and upper limits of the reference signal, respectively. ΔV represents the voltage ripple due to hysteresis. The expressions for $v_{A,min}$ and $v_{A,max}$ are defined as:

$$v_{A,min} = v_A(t) - \Delta V \tag{7}$$

$$v_{A,max} = v_A(t) + \Delta V \tag{8}$$

The aim of the UPFC is to maintain a constant load voltage (V_{L2}). Consequently, the reference signal can be adjusted according to the following:

$$v_A(t) = v_{L2}(t) - v_{abc}(t) \tag{9}$$

where $v_{abc}(t)$ signifies the desired load voltage. Consequently, the switching conditions are redefined as follows:

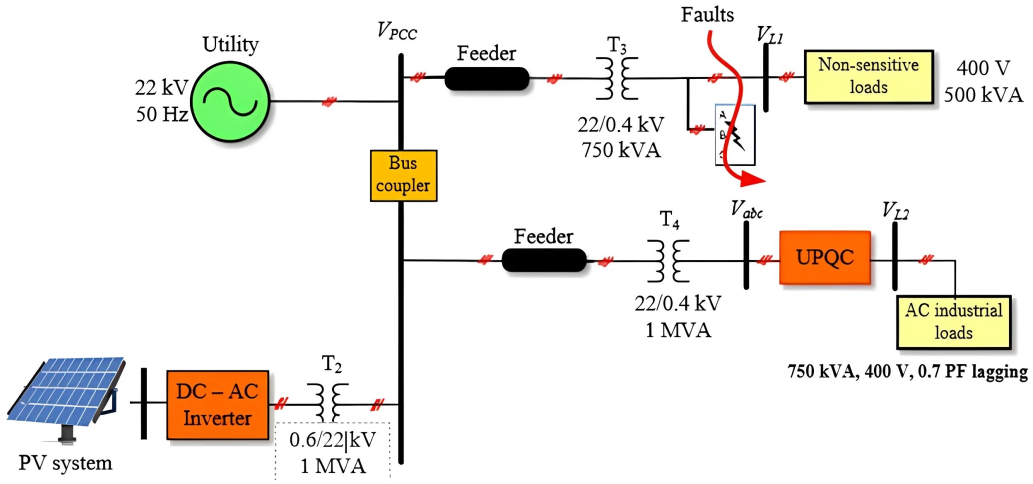

Fig. 1: Single-line diagram of UPFC–connected industrial distribution system.

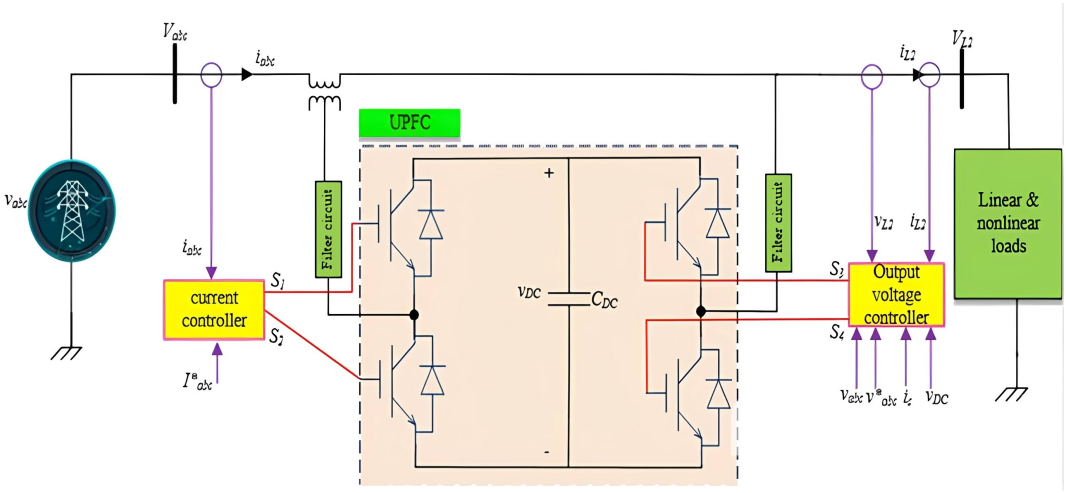

Fig. 2: UPFC structure.

Switching conditions for S_3 = on and S_4 = off:

$$v_L(t) - v_{L,min} - \left[\frac{k_A}{\frac{v_{DC}}{2} - v_L(t) + v_{abc}}\right] i_C^2(t) \leq 0 \quad (10)$$

$$i_C(t) \leq 0 \quad (11)$$

Switching conditions for S_3 = off and S_4 = on:

$$v_L(t) - v_{L,max} + \left[\frac{k_A}{\frac{v_{DC}}{2} + v_L(t) - v_{abc}}\right] i_C^2(t) \geq 0 \quad (12)$$

$$i_C(t) \geq 0 \quad (13)$$

$$v_{L,min} = v_{L2}(t) - \Delta V \quad (14)$$

$$v_{L,max} = v_{L2}(t) + \Delta V \quad (15)$$

The switching conditions can be illustrated clearly in Figure 3.

3.2. Series controller

The control strategy of the UPQC's-series DVR is illustrated in Fig. 4. The FOPID controller adjusts the DC link voltage within the exterior voltage control loop. Inside the control system, hysteresis control is employed in the internal loop to judge the input current against a reference signal generated by both the exterior loop and a phase-locked loop (PLL). This reference signal is utilized within the internal loop to ascertain the input current.

3.3. FOPID controller design

The performance of the system's transitory time response is demonstrated by evaluating the Fractional Order PIλDμ controller using a PQ evaluator. The presence of additional tuning knobs, such as the λ order integrator and μ order differentiator, enhances the

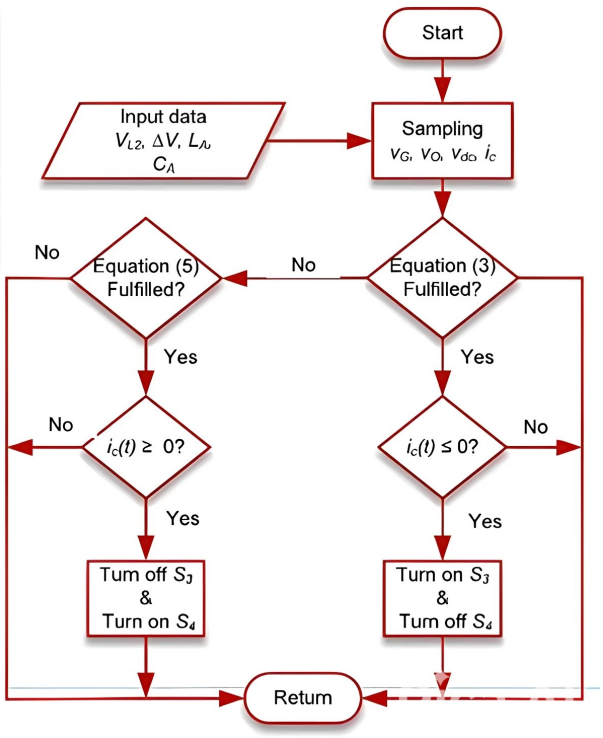

Fig. 3: Switching conditions for UPFC's-SPF.

effectiveness of the FOPID in steadying the changing aspects [40]. To evaluate the proposed approach, the Integral Time Absolute Error (ITAE) performance error index (Eq. 16) is chosen. This objective function is utilized to examine the effectiveness of the FOPID in an interrupted voltage situation.

$$ITAE = \int_0^{T_s} t \cdot |V_{dq0}(t)| dt \tag{16}$$

Where $V_{dq0}(t)$ denotes the error voltage. The time drawn for modelling is denoted by t.

The suggested method employs five coefficients and is articulated in both the time domain and Laplace domain as:

$$V_D(t) = [K_p + K_i D^{-\lambda} + K_d D^{\mu}] V_{dq0}(t), \quad (\lambda, \mu > 0) \tag{17}$$

$$P_c(s) = \frac{V_D(s)}{V_{dq0}(s)} = K_p + K_i s^{-\lambda} + K_d s^{\mu} \tag{18}$$

In equation (18), the controller output is represented by the variables $V_{dq0}(s)$ and $V_D(s)$, respectively. The remaining variables in the equation are K_p, K_i, K_d, λ, and μ. These gain parameters align with the proportional, integral, derivative, and fractional order aspects of the integral and differentiator functions.

4. Problem formulation

4.1. Objective function

This study employs two crucial objective functions in addressing power quality concerns within the power grid: THD and the voltage drop at network buses.

The expression of the fitness function of minimizing THD is as follows [24]:

$$f_1(X) = \min \left(\frac{1}{V_1} \sqrt{\sum_{h=2}^{\infty} V_h^2} \right) \tag{19}$$

Here, THDtotal and THDbusi represent the overall network THD and the THD at the i-th bus, respectively. Mitigating deviations in bus voltage, represented by dvoltage(X), from the reference value stands as a critical concern in distribution networks. This objective is addressed to enhance the voltage quality, ensure safe operations within the utility, and minimize the specified objective function as secondary objectives. The following equation is employed to reduce bus voltage drop:

$$f_2(X) = \max(|1 - V_{min}|, |1 - V_{max}|) \tag{20}$$

4.2. Constraints

The following limits employ to the optimization problem are as follows:

The voltage level is given by Eq. (21), thus.

$$0.95 \leq V_L \leq 1.05 \tag{21}$$

The THD_v and THD_i are given by Eq. (22), [41] thus.

$$THD_v \leq THD_{v,max} \tag{22}$$

4.3. Zebra Optimization Algorithm (ZOA)

The fundamental concept underlying the proposed ZOA design is inspired by the algebraic modelling of the smart behaviors demonstrated through zebras [42]. Each zebra can be viewed as a potential alternative to the problem in a statistical context, with their habitat symbolizing the search space of the issue. The position of each zebra within this search space reflects the values of the decision variables. Consequently, it can be depicted each zebra in the ZOA with a vector, where the vector's components correspond to the problem's variables. The zebra index can be mathematically represented using a matrix. Initially, the zebras' positions

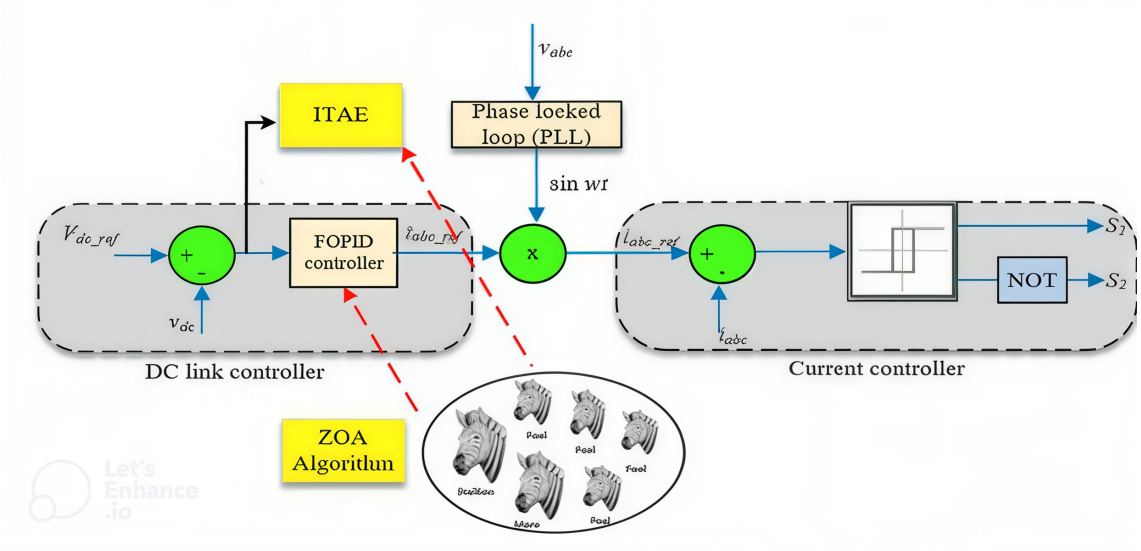

Fig. 4: Control circuit of UPFC's-DVR.

in the search space are randomly assigned. ZOA's population matrix is defined in Equation (23). Here, X represents the zebra population, Xi denotes an individual zebra, N is the zebra population, m signifies the number of decision variables, and Xi,j indicates the proposed value for the jth variable through the ith zebra.

$$X = \begin{bmatrix} X_1 \\ \vdots \\ X_i \\ \vdots \\ X_N \end{bmatrix}_{N\times m} = \begin{bmatrix} X_{1,1} & \cdots & X_{1,j} & \cdots & X_{1,m} \\ \vdots & \ddots & \vdots & \ddots & \vdots \\ X_{i,1} & \cdots & X_{i,j} & \cdots & X_{i,m} \\ \vdots & \ddots & \vdots & \ddots & \vdots \\ X_{N,1} & \cdots & X_{N,j} & \cdots & X_{N,m} \end{bmatrix}_{N\times m} \tag{23}$$

Using (24), a vector is used to represent the goal function's values.

$$F = \begin{bmatrix} F_1 \\ \vdots \\ F_i \\ \vdots \\ F_N \end{bmatrix}_{N\times 1} = \begin{bmatrix} F(X_1) \\ \vdots \\ F(X_i) \\ \vdots \\ F(X_N) \end{bmatrix}_{N\times 1} \tag{24}$$

The ZOA numbers undergo modification in two separate phases within every iteration. These phases consist of predator defense strategies and foraging activities. In the initial phase, population members are updated by mimicking zebras' foraging behaviors. The leading zebra within the group, referred to as the pioneer zebra, directs the remaining population towards its position within the search region. Equations (25) and (26) can be employed to mathematically represent the foraging phase.

$$x_{ij}^{new,P1} = x_{ij} + r(PZ_j - Ix_{ij}) \tag{25}$$

$$X_i = \begin{cases} X_i^{new,p1}, & F_i^{new,p1} < F_i \\ X_i, & \text{else} \end{cases} \tag{26}$$

Following the initial phase, the updated status of the ith zebra is denoted by $X_i^{new,p1}$.

Here, the value of its objective function is represented by $F_i^{new,p1}$ and the value of its jth dimension is represented by $x_{ij}^{new,P1}$. With its jth dimension denoted by PZj, the pioneer zebra, the top member, is recognized as PZ. The variable r represents a random number in the interval [0, 1]. I = round(1 + rand) as well. The second step simulates and uses the zebra's protection system against predator assaults. Depending on the kind of predator they face, zebras employ different protection mechanisms. It is considered that there is an equal chance of either of two outcomes:

i. The zebra chooses an escape route after being attacked by a lion. A mathematical model for this event may be found in (27) in the mode S1.

ii. When confronted with predators other than lions, the zebra will adopt an aggressive stance. This zebra approach is theoretically modeled using the mode S2, which is given in equation (27).

When a zebra adjusts its location, the new location is approved only if it results in an improvement in the objective function's value. Equation (28) defines the

criteria for this updating process.

$$x_{ij}^{new,P2} = \begin{cases} S_1 : x_{ij} + R(2r-1)(1-\frac{t}{T})x_{ij}, \\ \quad P_s \leq 0.5; \\ S_2 : x_{ij} + r(AZ_j - Ix_{ij}), \\ \quad \text{else} \end{cases} \tag{27}$$

$$X_i = \begin{cases} X_i^{new,p2}, & F_i^{new,p2} < F_i \\ X_i, & \text{else} \end{cases} \tag{28}$$

$X_i^{new,p2}$ represents the updated status of the ith zebra during the second phase, where $x_{ij}^{new,P2}$ signifies the value of its jth dimensions. The objective function can be denoted by $F_i^{new,p2}$, with t indicating the iteration number. The constant R is set at 0.01, T represents the maximum number of iterations, and P_s denotes the probability of randomly selecting one of two methods within the range [0, 1]. Furthermore, AZ describes the state of the zebra that encountered an attack, while AZ_j indicates the value of its jth dimension. Population membership undergo updates based on the first and second levels at the conclusion of every ZOA iteration. Upon the full implementation of the algorithm, population updates are executed according to equations (25) through (28). Iterations are iterated, with updates and the best candidate solution being preserved. Following the complete application of ZOA, the finest candidate solution provided stands as the optimal solution to the given problem.

4.4. Implementation of ZOA approach with the problem formulation

The flowchart of the ZOA approach is displayed in Fig. 5. The pseudocode for ZOA steps pertaining to the UPFC device's FOPID controller settings is provided by Method 1.

Method 1.

Input: The upper and lower bounds of FOPID controller parameters.

Put parameters of N and T.

Assemble the beginning population randomly.

For each zebra:

Estimate the objective function (minimize voltage drop and THD).

Check for constraints.

For $t = 1$ to T:

Pioneer zebras should be renewed.

For $i = 1$ to N:

Phase 1: Use (18) to determine the new state of the ith zebra. To update the ith zebra, use (26).

Make sure the modified size and location adhere to the restrictions.

Phase 2: $P_s = \text{rand}$, if $P_s < 0.5$

First strategy: lion assault.

In (27), use mode S_1 to determine the new state of the ith zebra.

Alternative 2: predators besides lions.

In (27), use mode S_2 to determine the new state of the ith zebra.

To update the ith zebra, use (21).

Make sure the revised size and location adhere to the limitations.

End for $i = 1$ to N.

Save the best possible solution thus far.

End for $t = 1$ to T.

Output: ZOA's optimal FOPID parameters solution.

Finish ZOA.

4.5. Setting of presented FOPID employing ZOA approach

Table 1 illustrates the optimal gains obtained for FOPID using the ZOA optimization approach. Three operations are examined for the simulation model: three diverse sorts of faults, balanced sag/swell, and unbalanced sag/swell.

5. Results and Discussion

Different varying operational conditions and harmonic analysis are utilized to evaluate the control methodologies. The outcomes on the load side are showcased, encompassing simulations both with and without the recommended UPFC. Furthermore, a comparison is drawn between the optimal UPFC performance using the current method and the most effective solution for fine-tuning the gains of optimized FOPID controllers. These evaluations are conducted using the MATLAB Simulink platform.

5.1. Off-grid PV Operation mode

The UPFC extracts voltage from the DC link capacitor and supplies it to the system to sustain the load volt-

Tab. 1: ZOA method for estimating the FOPID's optimum controller gains.

Control variables	Min Value	Max value	Event 1: Balanced voltage sag and swell	Event 2: Unbalanced voltage sag and swell	Event 3: fault condition
K_p	0	10	4.0460	3.1144	3.9013
K_i	0	5	2.2558	2.3364	1.6410
K_d	0	2	0.518	0.651	0.316
λ	0	2	1.669	1.745	1.580
μ	0	2	0.132	0.298	0.560

age at 380 Vrms. When the PV radiation decreases from 1000 W/m^2 to 800 W/m^2, causing the voltage to drop by 70% of its RMS value from 0.5s to 1.2 s, respectively, the system compensates accordingly. Figure 6 illustrates the grid, injected, and load voltages post-compensation. In addition, the UPFC system ensures the lower harmonics voltage by supporting with the compensating value. This, in turn, minimizes the THD from 9.34 to 1.9% in off-grid mode.

5.2. Event 1: Balanced and unbalanced sag

Figure 7 displays the ability of UPFC to mitigate unbalanced sag (80% of nominal voltage) from the period between (0.1 and 0.3 seconds) and balanced sag (70% of nominal voltage) from the period between (0.3 and 0.5 seconds) by introducing the appropriate voltage for maintaining a steady terminal voltage.

5.3. Event 2: Balanced swell

Figure 8 displays the ability of UPFC to mitigate balanced swell (140% of nominal voltage) from the period between (0.3 and 0.4 seconds) by introducing the appropriate voltage for maintaining a steady terminal voltage.

5.4. Event 3: Unbalanced sag and swell

Figure 9 shows the ability of UPFC to mitigate unbalanced sag from the period between (0.1 and 0.2 seconds) and unbalanced swell from the period between (0.3 and 0.4 seconds) by introducing the appropriate voltage for maintaining a steady terminal voltage.

5.5. Event 3: Fault conditions

Figure 10 shows the ability of UPFC to mitigate diverse faults of symmetrical faults on the first feeder from 0.2 to 0.35 s. The UPFC introduces the appropriate voltage at VL2 for maintaining a steady terminal voltage.

5.6. Assessment of harmonic distortions

The level of harmonic distortion in voltage or current waveforms can be accurately determined by measuring the THD [43]. Therefore, in this study, the THDv values at both the grid and load buses were examined using the presented UPFC-FOPID.

To assess the effectiveness of the UPFC-FOPID topology, Figure 11 illustrates the evaluated THDv at the load bus VL2 before and after compensation under various operating circumstances. The results clearly demonstrate a substantial reduction in THD values for both voltage and current, bringing them within the permissible bounds specified in IEEE 519 [44].

In addition, the UPFC system ensures the lower harmonics voltage by supporting with the compensating value, as depicted in Fig. 11. This, in turn, minimizes the THD from 12.09 to 1.84% in sag mode, as depicted in Fig. 11(a) and (b). Also, THD is minimized from 8.96% to 1.73% in swell mode, as depicted in Fig. 11(c) and (d). Furthermore, THD is minimized from 9.32% to 2.00% in fault conditions, as depicted in Fig. 11(e) and (f).

5.7. Comparative assessments

This section presents two comparative investigations of various optimizations and another controller aimed at enhancing the efficiency and resilience of the UPFC scheme.

To imitate the performances of the proposed UPFC typology, the FOPID controller utilizes the ZOA method, along with whale optimization algorithm (WOA) [45] and the PSO [46]. Table 2 illustrates a comparative study of these three algorithms specifically in the context of on-grid operation mode, aligning

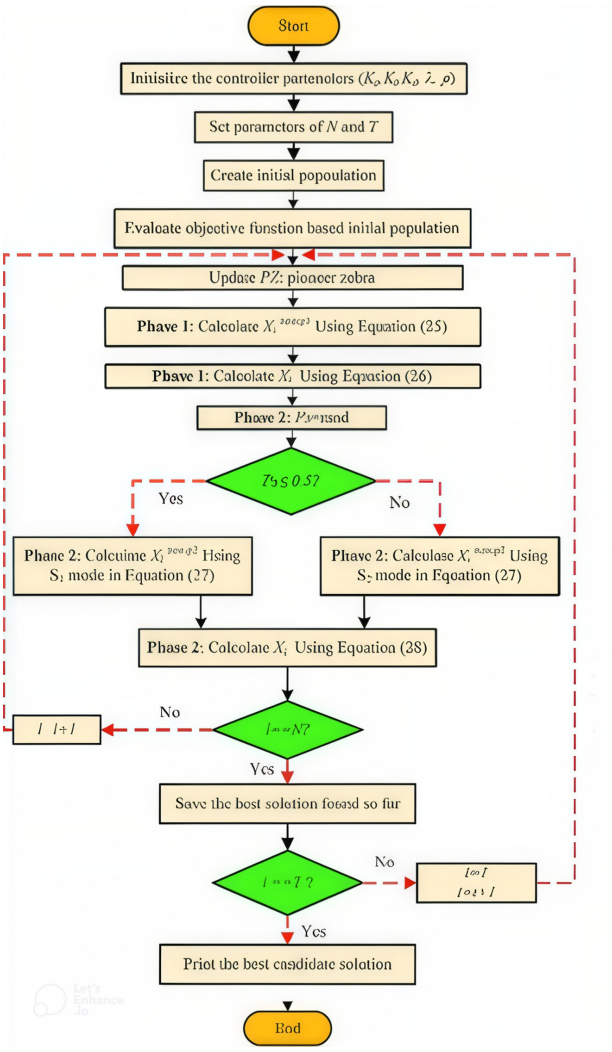

Fig. 5: ZOA flowchart.

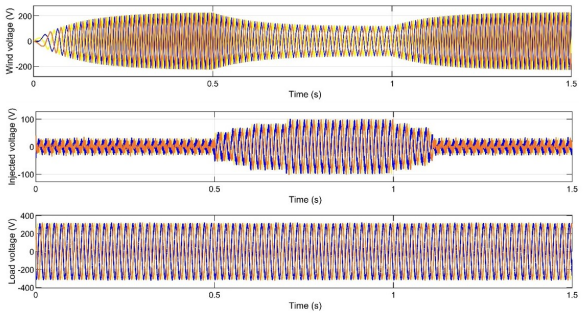

Fig. 6: Changes in the PV radiation and its impact on the grid voltage, injected voltage, and load voltage.

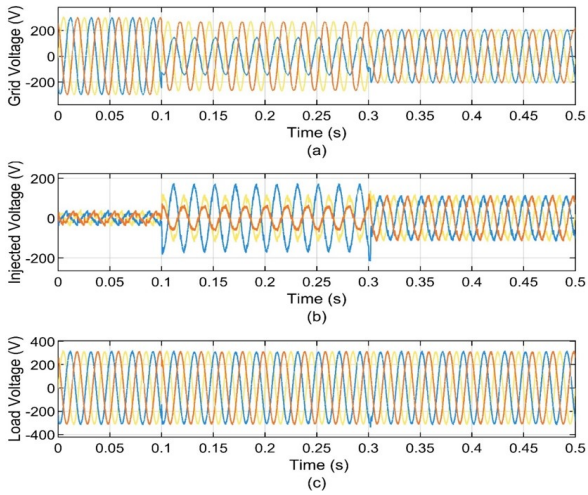

Fig. 7: Simulation findings of UPFC performance for voltage sag; V_{abc}, V_{inj}, V_{L2}.

with the objectives of the proposed typology. The results consistently demonstrate that ZOA achieves the best fitness values with the minimum number of trials and the low computational time. Also, the proposed ZOA has two control parameters in comparison with other optimizations.

The data clearly indicates that ZOA consistently and reliably impacts the optimum values of the objective function per the minimum iterations required.

6. Conclusion

In this research, a study was conducted on renewable sources of wind turbines operating in various conditions. These conditions were analyzed with the existence of nonlinear loads, which posed power quality (PQ) issues such as voltage dips, swells, fault conditions, and harmonics. To face these issues, a unified power flow controller (UPFC) is employed. The control of the UPFC was attained using an FOPID control strategy with the improved zebra optimization algorithm (ZOA) to get the appropriate gain values for different PQ problems.

Furthermore, three comparative studies were carried out. The first study compared diverse optimizations with the presented UPFC approach. The results showed that the proposed ZOA approach in three events yielded the shortest computing time of 173.554, 257.544, and 382.405 seconds and achieved an objective function value of 2.371, 2.387, and 2.398, respectively. These outcomes represented significant improvements over other optimization methods. In the second comparative study, an alternative controller called PID was evaluated with the proposed FOPID controller during operating grid conditions. The obtained results demonstrated that the UPFC-FOPID controller exhibited excellent performance in regards to its rapid response and minimized fitness function.

Overall, the results of this work indicated that the optimal UPFC-FOPID control technique successfully addressed voltage superiority performance and har-

Tab. 2: Comparative investigation of the same FOPID controller with diverse optimizations.

Optimization approaches	**PSO**	**WOA**	**Presented (ZOA)**
Max. iteration	270	270	270
Search agent	20	20	20
Computation time (s)	382.405	257.544	173.554
$f_1(\%)$	4.12	4.01	1.84
f_2	2.398	2.387	2.371
Control parameters	w, m, C_1, C_2 & v_{max}	C_{max}= 1 & C_{min}= 0.00004	σ & C_1
K_p	3.896	3.398	4.0460
K_i	2.6145	2.472	2.2558
K_d	0.5872	0.532	0.518
λ	1.3365	1.461	1.669
μ	0.1985	0.338	0.132
V_{L2} (pu)	0.9575	0.9741	0.9921
I_{L2} (pu)	0.6347	0.6354	0.4792
P (pu)	0.5712	0.5818	0.4469
Q (pu)	0.2066	0.2104	0.1616

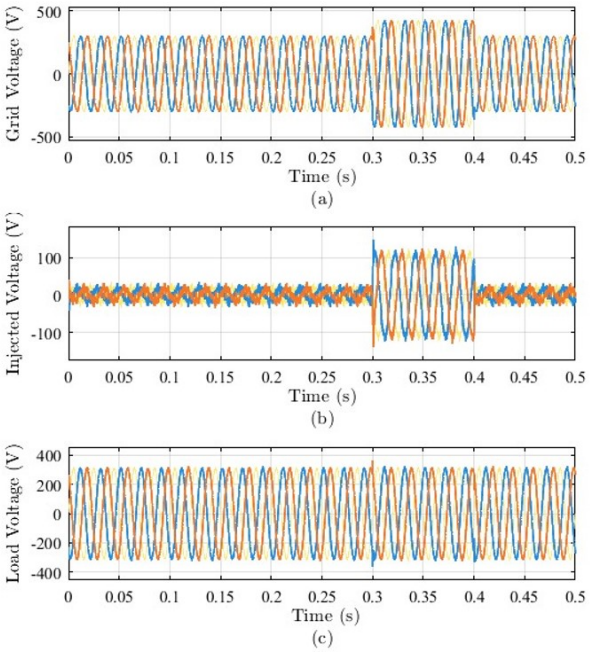

Fig. 8: Simulation findings of UPFC performance for voltage swell; V_{abc}, V_{inj}, V_{L2}.

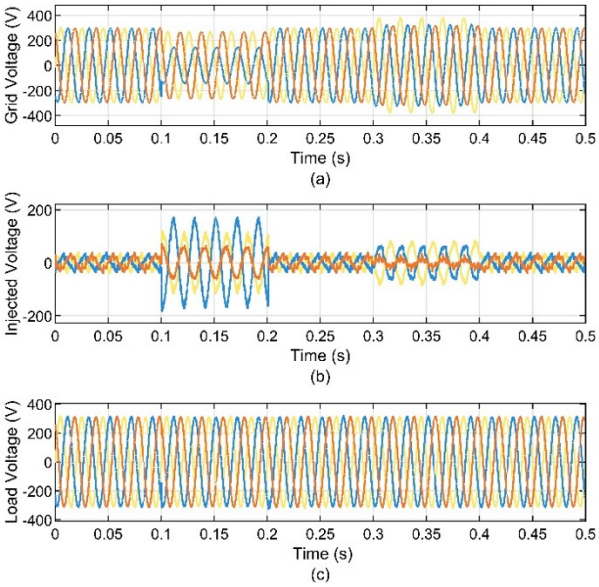

Fig. 9: Simulation findings of UPFC performance for unbalanced voltage sag and swell; V_{abc}, V_{inj}, V_{L2}.

monic elimination when confronted with grid voltage alterations.

Finally, the potential challenges and limitations of implementing the proposed UPFC control strategy with ZOA optimization in large-scale power systems or grid-integrated renewable energy setups can be briefed as follows:

1- Implementing the UPFC management method with ZOA optimisation in large-scale power systems or grid-integrated renewable energy configurations may provide problems and limits, including scalability concerns. As electricity systems become more sophisticated and large, the computational demands on the ZOA may rise, making it harder to maintain efficiency and timeliness.

2- Unpredictability in renewable energy sources causes rapid fluctuations in demand and generation for

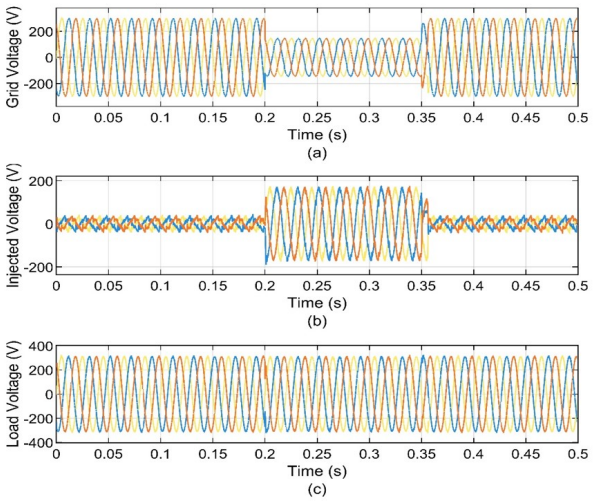

Fig. 10: Simulation findings of UPFC performance for fault conditions; V_{abc}, V_{inj}, V_{L2}.

large-scale systems. The control approach must be robust enough to adapt to these dynamic conditions in real-time, which may be difficult to do.

3- In grid-integrated settings, many UPFC devices may need to work together to ensure synchronised functioning. This demands a permanent communication setup, which can be complicated in significantly distributed systems.

4- The cost-efficiency of implementing UPFCs with the ZOA approach in large-scale systems has to be demonstrated. High initial investment and ongoing maintenance costs may limit the feasibility of widespread utilization.

Author Contributions

A. M. M.: Conceptualization, Methodology, Writing-Original draft preparation; G. A. M.: Data curation, Visualization, Investigation; H. A. K.: Resources, Validation; R. A. A.: Software, Writing -Review & amp; Editing, Supervision.

References

[1] BABAYOMI, O., Y. LI, Z. ZHANG, K.-B. PARK. Advanced Control of Grid-Connected Microgrids: Challenges, Advances, and Trends. *IEEE Transactions on Power Electronics*. 2025, vol. 40, no. 6, pp. 7681-7708. DOI: 10.1109/TPEL.2025.3526246.

[2] MOUSAEI, A., M. GHEISARNEJAD, M. H. KHOOBAN. Challenges and opportunities of FACTS devices interacting with electric vehicles in distribution networks: A technological review. *Journal of Energy Storage*. 2023, vol. 73. DOI: 10.1016/j.est.2023.108860.

[3] EROĞLU, H., O. KURTULUŞ, O. CAN. Decision making methods used for improving power quality to meet the sustainable energy targets. *Energy & Environment*. 2024, vol. 36, iss. 1, pp. 499-539. DOI: 10.1177/0958305X241276829.

[4] BIN ABU SOFIAN, A. D. A., et al. Machine learning and the renewable energy revolution: Exploring solar and wind energy solutions for a sustainable future including innovations in energy storage. *Sustainable Development*. 2024, vol. 32, no. 4, pp. 3953–3978. DOI: 10.1002/sd.2885.

[5] GUPTA, A., K. K. SHARMA, G. KAUR. Integrated Electric Power Systems and Their Power Quality Issues. *Power Electronics for Green Energy Conversion*. 2022. DOI: 10.1002/9781119786511.ch2.

[6] SAHOO, S. Chapter 12 - Recent trends and advances in power quality. *Power Quality in Modern Power Systems*. 2021, pp. 337–358. DOI: 10.1016/B978-0-12-823346-7.00010-4.

[7] ALAJRASH, B. H., et al. A comprehensive review of FACTS devices in modern power systems: Addressing power quality, optimal placement, and stability with renewable energy penetration. *Energy Reports*. 2024, vol. 11, pp. 5350–5371. DOI: 10.1016/j.egyr.2024.05.011.

[8] HERNÁNDEZ-MAYORAL, E., et al. A Comprehensive Review on Power-Quality Issues, Optimization Techniques, and Control Strategies of Microgrid Based on Renewable Energy Sources. *Sustainability*. 2023, Vol. 15, no. 12. DOI: 10.3390/su15129847.

[9] TRAN, D. T., A.-T. TRAN, V. VAN HUYNH, T. D. DO. Decentralized Frequency Regulation by Using Novel PID Sliding Mode Structure in Multi-Area Power Systems With Hydropower Turbines. *IEEE Access*. 2025, vol. 13, pp. 18850–18862. DOI: 10.1109/ACCESS.2025.3532516.

[10] TRAN, A.-T., M. P. DUONG, N. T. PHAM, J. W. SHIM. Enhanced sliding mode controller design via meta-heuristic algorithm for robust and stable load frequency control in multi-area power systems. *IET Generation, Transmission & Distribution*. 2024, vol. 18, pp. 460–478. DOI: 10.1049/gtd2.13077.

[11] TRAN, A.-T., N. T. PHAM, V. Van HUYNH, D. N. M. DANG. Stabilizing and Enhancing

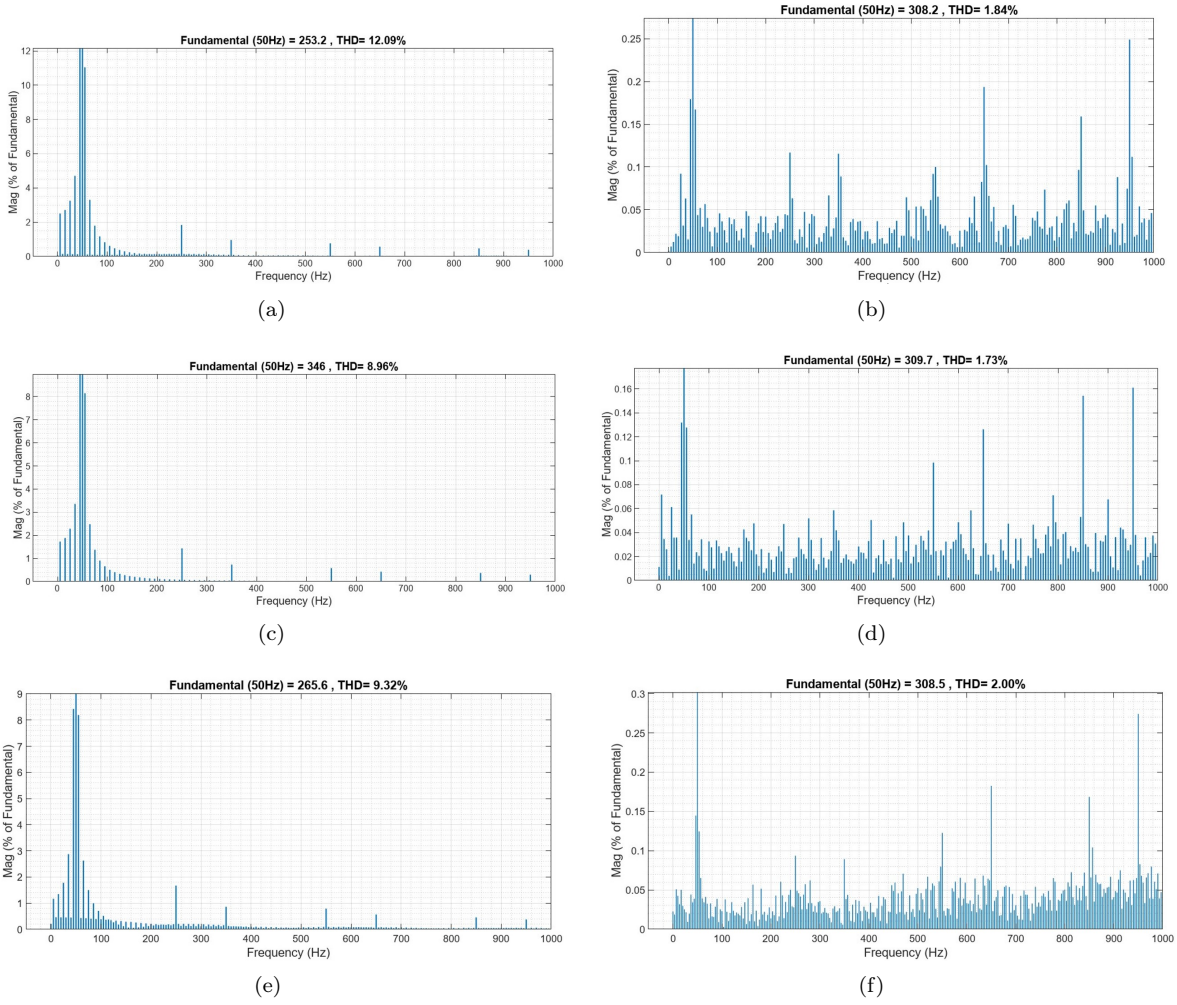

Fig. 11: THD of the voltages at V_{L2}: (a) without UPFC during sag event, (b) with UPFC during sag event, (c) without UPFC during swell event, (d) with UPFC during swell event, (e) without UPFC during fault event, (f) with UPFC during fault event.

Frequency Control of Power System Using Decentralized Observer-Based Sliding Mode Control. *Journal of Control, Automation and Electrical Systems*. 2023, vol. 34, no. 3, pp. 541–553. DOI: 10.1007/s40313-022-00979-y.

[12] JUMANI, T. A., et al. Swarm Intelligence-Based Optimization Techniques for Dynamic Response and Power Quality Enhancement of AC Microgrids: A Comprehensive Review. *IEEE Access*. 2020, vol. 8, pp. 75986-76001. DOI: 10.1109/ACCESS.2020.2989133.

[13] JUMANI, T. A., et al. Computational Intelligence-Based Optimization Methods for Power Quality and Dynamic Response Enhancement of ac Microgrids. *Energies*. 2020, vol. 13, no. 15. DOI: 10.3390/en13164063.

[14] MAROUANI, I., et al. Optimized FACTS Devices for Power System Enhancement: Applications and Solving Methods. *Sustainability*. 2023, vol. 15, no. 12. DOI: 10.3390/su15129348.

[15] EL-RAOUF, M. O. A., et al. Performance Enhancement of Grid-Connected Renewable Energy Systems Using UPFC. *Energies*. 2023, vol. 16, no. 11. DOI: 10.3390/en16114362.

[16] RAVI, T., K. S. KUMAR, C. DHANAMJAYULU, B. KHAN, K. RAJALAKSHMI. Analysis and mitigation of PQ disturbances in grid connected system using fuzzy logic based IUPQC. *Scientific Reports*. 2023, vol. 13. DOI: 10.1038/s41598-023-49042-z.

[17] SRILAKSHMI, K., et al. Optimal Design of an Artificial Intelligence Controller for Solar-Battery Integrated UPQC in Three Phase Distribution Networks. *Sustainability*. 2022, vol. 14, no. 21. DOI: 10.3390/su142113992.

[18] MAHABOOB, S., S. K. AJITHAN, S. JAYARAMAN. Optimal design of shunt active power filter for power quality enhancement using predator-prey based firefly optimization. *Swarm and Evolutionary Computation*. 2019, vol. 44, pp. 522–533. DOI: 10.1016/j.swevo.2018.06.008.

[19] JAWAD, R., R. JAWAD, Z. SALMAN. Ant Colony Algorithm (ACO) Applied for Tuning PI of Shunt Active Power Filter (SAPF). *Iraqi Journal for Electrical And Electronic Engineering*. 2021, vol. 17, iss. 2 pp. 204–211. DOI: 10.37917/ijeee.17.2.23.

[20] SINGH, B., R. KUMAR. A comprehensive survey on enhancement of system performances by using different types of FACTS controllers in power systems with static and realistic load models. *Energy Reports*. 2020, vol. 6, pp. 55–79. DOI: 10.1016/j.egyr.2019.08.045.

[21] GEORGILAKIS, P. S., N. D. HATZIARGYRIOU. Unified power flow controllers in smart power systems: models, methods, and future research. *IET Smart Grid*. 2019, vol. 2, pp. 2–10. DOI: 10.1049/iet-stg.2018.0065.

[22] PHAN, D., et al. Neuro-Fuzzy System for Energy Management of Conventional Autonomous Vehicles. *Energies*. 2020, vol. 13, no. 7. DOI: 10.3390/en13071745.

[23] RAJESH, P., F. H. SHAJIN, L. UMASANKAR. A Novel Control Scheme for PV/WT/FC/Battery to Power Quality Enhancement in Micro Grid System: A Hybrid Technique. *Energy Sources, Part A: Recovery, Utilization and Environmental Effects*. 2021, pp. 1-17. DOI: 10.1080/15567036.2021.1943068.

[24] ARUNSANKAR, G., S. SRINATH. Optimal controller for mitigation of harmonics in hybrid shunt active power filter connected distribution system: An EGOANN technique. *Journal of Renewable and Sustainable Energy*. 2019, vol. 11, iss. 2. DOI: 10.1063/1.5085028.

[25] RAMADEVI, A., et al. Optimal Design and Performance Investigation of Artificial Neural Network Controller for Solar- and Battery-Connected Unified Power Quality Conditioner. *International Journal of Energy Research*. 2023. DOI: 10.1155/2023/3355124.

[26] SAID, A., et al. Support Vector Machine Parameters Optimization for 500 kV Long OHTL Fault Diagnosis. *IEEE Access*. 2023, vol. 11, pp. 3955–3969. DOI: 10.1109/ACCESS.2023.3235592.

[27] MOHSEN, S. E. A., A. M. IBRAHIM, Z. M. S. ELBARBARY, A. I. OMAR. Unified Power Quality Conditioner Using Recent Optimization Technique: A Case Study in Cairo Airport, Egypt. *Sustainability*. 2023, vol. 15, no. 4. DOI: 10.3390/su15043710.

[28] OMAR, A. I., et al. Induced Overvoltage Caused by Indirect Lightning Strikes in Large Photovoltaic Power Plants and Effective Attenuation Techniques. *IEEE Access*. 2022, vol. 10, pp. 112934–112947. DOI: 10.1109/ACCESS.2022.3216866.

[29] SAID, A., M. A. ABD-ALLAH, M. MOHSEN, A. I. OMAR. Alleviation of the transients induced in large photovoltaic power plants by direct lightning stroke. *Ain Shams Engineering Journal*. 2023, vol. 14, iss. 3. DOI: 10.1016/j.asej.2022.101880.

[30] ADAIKKAPPAN, M., et al. Arithmetic optimization based MPPT for photovoltaic systems operating under nonuniform situations. *PLoS ONE*. 2024. vol. 19, no. 12. DOI: 10.1371/journal.pone.0311177.

[31] HASSAN, A. M., et al. MPPT control of a solar pumping system based five-phase impedance source inverter fed induction motor. *PLoS ONE*. 2024, vol. 19, no. 1. DOI: 10.1371/journal.pone.0295365.

[32] IBRAHIM, N. F., et al. A new adaptive MPPT technique using an improved INC algorithm supported by fuzzy self-tuning controller for a grid-linked photovoltaic system. *PLoS ONE*. 2023, vol. 18, no. 11. DOI: 10.1371/journal.pone.0293613.

[33] HASSAN, A. T., et al. Adaptive Load Frequency Control in Microgrids Considering PV Sources and EVs Impacts: Applications of Hybrid Sine Cosine Optimizer and Balloon Effect Identifier Algorithms. *International Journal of Robotics and Control Systems*. 2024, vol. 4, no. 2, pp. 941–957. DOI: 10.31763/ijrcs.v4i2.1448.

[34] LAMINE, O. M., et al. A Combination of INC and Fuzzy Logic-Based Variable Step Size for Enhancing MPPT of PV Systems. *International Journal of Robotics and Control Systems*. 2024, vol. 4, no. 2, pp. 877–892. DOI: 10.31763/ijrcs.v4i2.1428.

[35] HAMID, M. N. A., et al. Adaptive Frequency Control of an Isolated Microgrids Implementing Different Recent Optimization Techniques. *International Journal of Robotics and Control Systems*. 2024, vol. 4, no. 3, pp. 1000–1012. DOI: 10.31763/ijrcs.v4i3.1432.

[36] RAJ, A., et al. Wavelet Analysis- Singular Value Decomposition Based Method for Precise Fault Localization in Power Distribution Networks Using k-NN Classifier. *International Journal of Robotics and Control Systems*. 2025, vol. 5, no. 1, pp. 530–554. DOI: 10.31763/ijrcs.v5i1.1543.

[37] MOHSEN, S. E. A., A. M. IBRAHIM, A. I. OMAR. Robust Control of Unified Power Quality Conditioner for LED Lighting Using Enhanced Bald Eagle Search Optimization. *23rd International Middle East Power Systems Conference (MEPCON), Cairo, Egypt*. 2022, pp. 1-6. DOI: 10.1109/MEPCON55441.2022.10021737.

[38] MAHMOUD, M. M., et al. Application of Whale Optimization Algorithm Based FOPI Controllers for STATCOM and UPQC to Mitigate Harmonics and Voltage Instability in Modern Distribution Power Grids. *Axioms*. 2023, vol. 12, no. 5. DOI: 10.3390/axioms12050420.

[39] ELMETWALY, A. H., et al. Modeling, Simulation, and Experimental Validation of a Novel MPPT for Hybrid Renewable Sources Integrated with UPQC: An Application of Jellyfish Search Optimizer. *Sustainability*. 2023, vol. 15, no. 6. DOI: 10.3390/su15065209.

[40] ALDOSARY, A. Power Quality Conditioners-Based Fractional-Order PID Controllers Using Hybrid Jellyfish Search and Particle Swarm Algorithm for Power Quality Enhancement. *Fractal and Fractional*. 2024, vol. 8, no. 3. DOI: 10.3390/fractalfract8030140.

[41] SAKAR, S., M. E. BALCI, S. H. E. ABDEL ALEEM, A. F. ZOBAA. Integration of large-scale PV plants in non-sinusoidal environments: Considerations on hosting capacity and harmonic distortion limits. *Renewable and Sustainable Energy Reviews*. 2018, vol. 82, pp. 176–186. DOI: 10.1016/j.rser.2017.09.028.

[42] TROJOVSKÁ, E., M. DEHGHANI, P. TROJOVSKÝ. Zebra Optimization Algorithm: A New Bio-Inspired Optimization Algorithm for Solving Optimization Algorithm. *IEEE Access*. 2022, vol. 10, pp. 49445–49473. DOI: 10.1109/ACCESS.2022.3172789.

[43] HU, Z., et al. Harmonic Sources Modeling and Characterization in Modern Power Systems: A Comprehensive Overview. *Electric Power Systems Research*. 2023, vol. 218. DOI: 10.1016/j.epsr.2023.109234.

[44] HANAINEH, W. A., et al. A THD-Based Fault Protection Method Using MSOGI-FLL Grid Voltage Estimator. *Sensors*. 2023, vol. 23, no. 2. DOI: 10.3390/s23020980.

[45] OMAR, A. I., et al. An improved approach for robust control of dynamic voltage restorer and power quality enhancement using grasshopper optimization algorithm. *ISA Transactions*. 2019, vol. 95, pp. 110–129. DOI: 10.1016/j.isatra.2019.05.001.

[46] JEYARAJ, K., D. DEVARAJ, A. I. S. VELUSAMY. Development and performance analysis of PSO-optimized sliding mode controller–based dynamic voltage restorer for power quality enhancement. *International Transactions on Electrical Energy Systems*. 2020, vol. 30. DOI: 10.1002/2050-7038.12243.